PERGAMON

International Journal of Heat and Mass Transfer 42 (1999) 1467–1478

International Journal of HEAT and MASS TRANSFER

Spray evaporation heat transfer of R-141b on a horizontal tube bundle

T.B. Chang, J.S. Chiou*

Mechanical Engineering Department, National Cheng Kung University, Tainan, Taiwan

Received 30 December 1997; in final form 17 June 1998

Abstract

The spray of R-141b coolant on a horizontal staggered tube bundle was used to investigate the performance of spray cooling heat transfer in a compact heat exchanger system. The test tube used in the present work is a 19.1 mm (3/4 inch) diameter copper tube, heated by an electrical resistor. The spray nozzle has a full cone shape with its hydraulic diameter at 2 mm. The average heat transfer coefficients were calculated by measuring the mean tube surface temperature and the vapor temperature. Pool boiling experiments were also conducted and compared with spray cooling data under the same test conditions. The dry-out phenomenon was observed once the surface heat flux approached the critical heat flux (CHF). In this study, a liquid film collector is specifically designed for each tube to prevent the dry-out phenomenon. The heat transfer performance for spray cooling with a liquid film collector was found to be much better than the performance of pool boiling under both low and high heat fluxes.

Key words: Impacting spray cooling; Boiling heat transfer; CHF

Nomenclature

A total surface area with power
D diameter of heater tube
h heat transfer coefficient
m spray mass flow rate
M molecular weight
n index defined in eq. (5)
P pressure
P_{cr} P/P_c
q'' wall heat flux
Q_h total power of heater
R_p surface roughness
T temperature.

Subscripts
c critical point value
s saturation state value
sur surrounding environment value
nb nucleate boiling.

1. Introduction

Recent emphasis on removing high heat fluxes from electronic devices [1] and neutral beam calorimeter and plasma limiters [2] requires the removal of surface heat to the limit. In conventional methods of forced convective and radiative heat transfer, high heat fluxes can be achieved by a large difference between the surface temperature and the flow temperature. However, such heat transfer modes entail excessively high surface temperatures, which could be detrimental to the heat transfer surface and system. The removal of the high density heat fluxes from a solid surface has been and will still be dependent on high velocity fluid flow and the phase change of coolant such as flow boiling heat transfer and impinging liquid jets [3]. Impinging spray cooling is the method which sprays liquid droplets directly on the heated surface.

Earlier investigations on directly impacting spray cooling have focused on the cases with surface temperatures above the Leidenfrost temperature, therefore film boiling conditions were usually observed, such as in the study performed by Hodgson and Sutherland [4]. Recently, Choi and Yao [5] and Pais et al. [6] conducted

* Corresponding author. Tel.: +886-6-275-7575; Fax: +886-6-235-2973; E-mail: jschiou@mail.ncku.edu.tw.

0017–9310/98/$ - see front matter
PII: S0017–9310(98)00214–0

spray cooling tests and explained that the high velocity liquid droplets could break up the liquid film on the solid surface and let the vapor bubble release more easily. The hydrodynamic instabilities inherent in pool boiling CHF could then be precluded.

In terms of fundamental descriptions of impacting sprays, there are many parameters which may play an important role in the overall hydrodynamics and heat transfer processes. These parameters including the physical properties of the sprayed liquid may vary significantly from case to case, such as the size of droplets, the droplet velocity and spray pattern (or nozzle pattern, for example either a solid cone or a hollow cone etc.). Deb and Yao [7] found the above mentioned droplet parameters might significantly influence the overall heat transfer results for the case with dilute spray but not for the case with dense spray. In dilute spray, they tried to delineate the heat transfer mechanism via three subprocesses which were: drop contact heat transfer, bulk air convective heat transfer and radiative heat transfer.

When a circular tube receives overhead spray, the upper surface of the tube is indeed subjected to impacting spray cooling, however, its bottom side does not receive any spray. In fact, the surface is covered by the falling liquid film. The heat transfer mode on the bottom surface of the horizontal tube is thus a film evaporation.

Chyu and Bergles [8–10] showed the film evaporative mode can provide a greater heat transfer coefficient than pool boiling mode at low heat flux on a plain surface. But in the high heat flux region, the thin liquid film will evaporate completely and the dry-out phenomenon would occur at the bottom surface. The heat transfer coefficient will suddenly drop once the dry-out phenomenon occurs. Moeykens and Pate [11] found a higher supply rate of refrigerant could somehow delay the dry-out phenomenon to occur. They also indicated that the performance of spray evaporation heat transfer on a horizontal plain tube was less than the performance of pool boiling at higher heat fluxes (if dry-out had occurred).

For a tube bundle, the overhead spray can barely reach the lower tubes. Moeyken and Pate [12] used four nozzles to spray the coolant on a triangular-pitch tube bundle with four rows of tubes. They found the heat transfer performance of the second and fourth rows (from top) is much less than that of the top and third rows. The reason behind this was that the tubes of the third row (located in-line below the top-row tubes) received more liquid dripping from the first row. On the other hand, there is less liquid to cool down the second and fourth row tubes. Therefore, the spray cooling is hardly used for tube bundles because the overall heat transfer performance is not necessary better than that of flooded cooling (cooled by pool boiling).

To take the advantage of spray cooling and eliminate its drawbacks on tube bundles such as the dry-out phenomenon occurring on the bottom side of the tube and poor cooling performance on the lower-row tubes, we designed a liquid collector to attach to each tube, see Fig. 1a. The liquid collectors can collect the liquid film falling along the circumference to prevent the dry-out on the bottom side of the tube, and the overfill liquid (the gap between the tube surface and collector is only 2 mm) will fall directly to the tube of the next row instead of the row further below, see Fig. 1b.

Most of the previous tests conducted to perform the evaporation heat transfer have been done with water, such as Chun and Seban [13], and Chyu et al. [14]. They used water as coolant to develop the falling film evaporation models and correlations. Recently, Thome reviewed the tests of two-phase heat transfer by using refrigerant as the cooling fluid [15], he commented the study of boiling heat transfer for tube bundles is very limited.

In this study, refrigerant R-141b which did not appear in Thome's reviewing list [15] is used as the working fluid in our experimental study. The results obtained in this work should be able to expand the data bank of boiling heat transfer performance.

2. Experimental facilities

The experimental facilities in the present work are able to measure the shell-side heat transfer coefficients in either a spray evaporation or a pool boiling mode. Figure 2 shows the test facilities including the refrigerant flow loop, the glycol/water flow loop, the test section, the spray nozzle, the tube bundle, and the data acquisition system. The detailed descriptions for the above components are presented in the followings.

2.1. Main flow loop

The main flow loop is a closed-type circulation loop, the function of this loop is to keep the liquid refrigerant entering the test section at a desired flow rate and at a desired temperature. A bypass valve is installed at the outlet of refrigerant pump to regulate the mass flow rate of the spray. The refrigerant mass flow rate is measured by a floating-type flow meter at the inlet of the test section, in the mean time, the temperature and pressure of inlet liquid must also be measured. In the test section, the liquid refrigerants are sprayed out from the nozzle, the spray impinges on the heated tube followed by the evaporation processes. The evaporated refrigerant (vapor) is guided into a condenser. The condensed liquid is merged with the non-evaporated liquid, the combined liquid mass flow rate and its temperature are measured before entering into the storage tank.

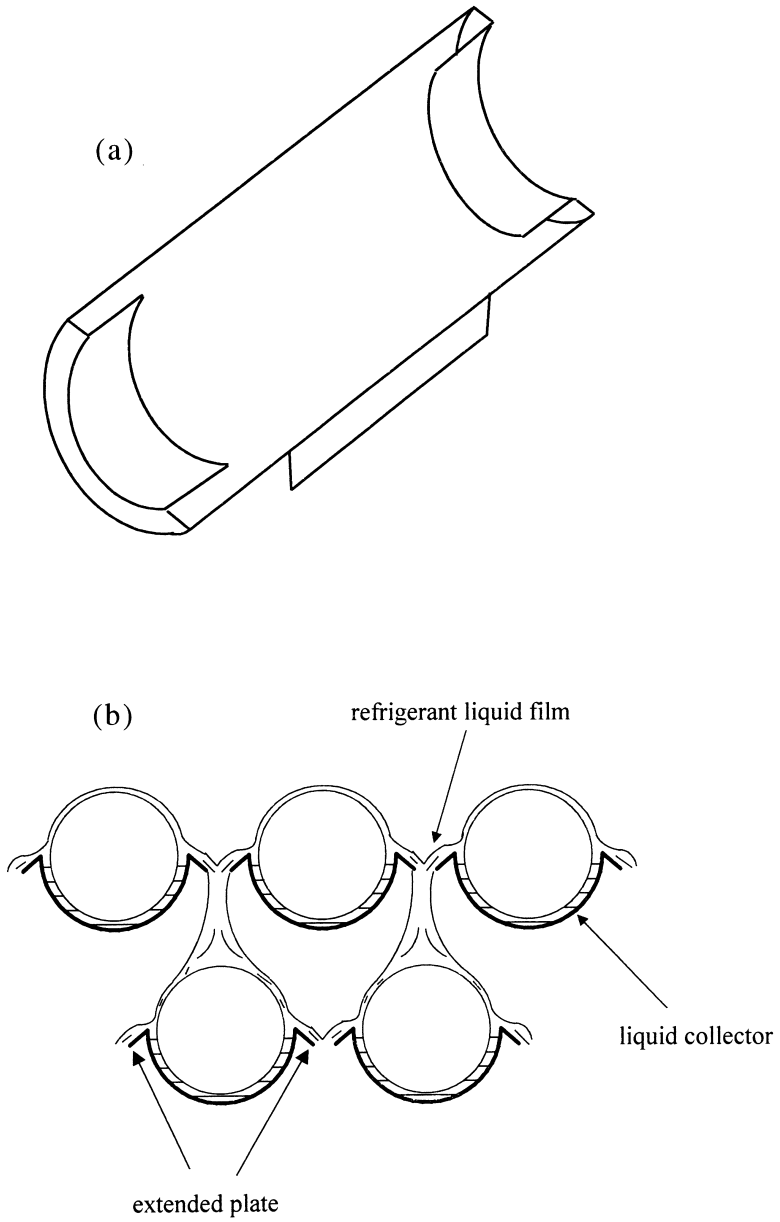

Fig. 1. (a) Schematic diagram of a liquid collector. (b) Test bundle tubes with liquid collectors.

2.2. Test section

The test section is made by stainless steel, its inner diameter is 20.2 cm and the length is 33.5 cm. The heater tubes are firmly fastened at one end of the two vertical side plates and tightly sealed on both side plates. In order to reduce the heat loss from the test section, the outer-surface of the test section was covered by a two inches layer of extruded cellular polyurethane. Two view-glass ports are designed for eye observation and for photography purposes. Along the upper side of the test section, there are two take-off pipes, one is the liquid inlet pipe and the other is the vapor outlet pipe. A thermocouple is installed in the test section to measure the refrigerant vapor temperature. A electrical pressure sensor is also installed in the test section to detect the

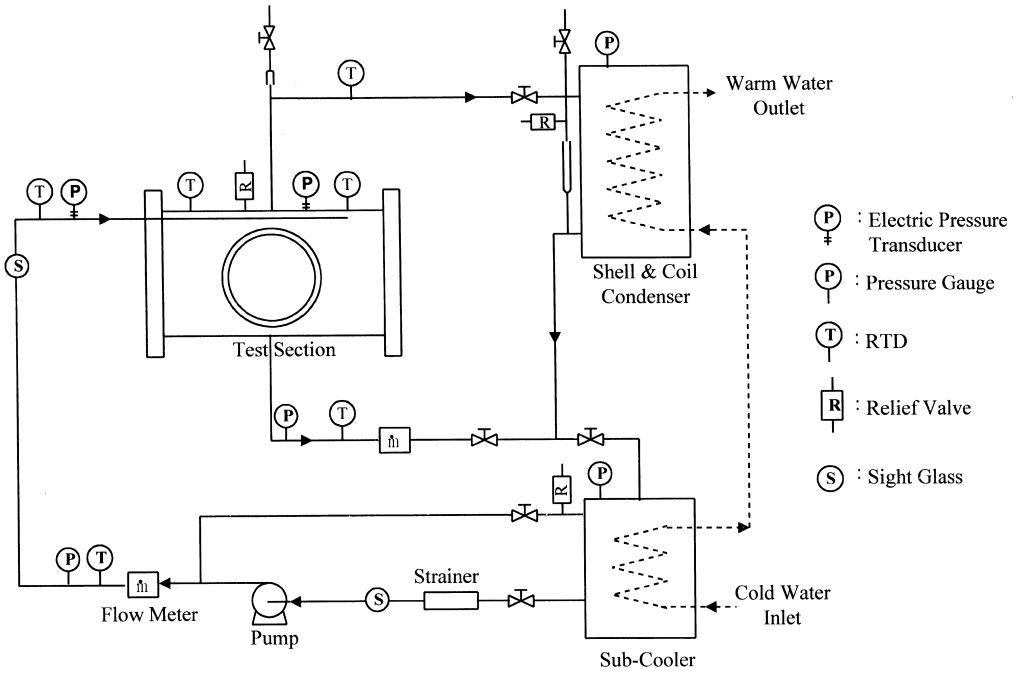

Fig. 2. Spray evaporation test rig.

stability of vapor pressure, from which the corresponding saturation temperature can then be obtained. At the bottom side of the test section, there is a liquid outlet which allows the non-evaporated liquid refrigerant to flow out and return back to the storage tank.

2.3. Spray nozzle

The spray nozzle is a full cone circular hydraulic nozzle with its orifice diameter at 2 mm. The liquid refrigerant is sprayed from the nozzle as liquid sheets and then disintegrate into many liquid droplets. The differential pressure across the nozzle determines the quantity of sprayed liquid, which can also be controlled by the liquid inlet valve.

2.4. Tube bundle

The heat source in the test section is provided by the resistor-type heater tubes which are fabricated by WATLOW with the code number of J10N-588. The heater tube with a power length of 20 mm and a diameter of 19.05 mm (3/4 inch) can emit the heat flux up to 700 kW/m^2 (222 040 Btu/h ft^2).

Figure 3a depicts the detailed schematic of a heater tube. The outer surface of the tube is made of copper. Three thermocouples were installed on the surface of each heater tube through drilled ports, which were filled with a lead–tin solder. The size of the drilled port was kept minimum so that the temperature of the solder bead would be as close as possible to the actual wall temperature. Thermocouple wires were run through the space between the outer surface of the cartridge heater and the inner surface of the copper tube. In order to maintain the cartridge heater in a centerline position within the copper tube, the space between the outside of the cartridge heater and the inside of the copper tube is filled with a mixture of magnesium dioxide powder and highly conductive grease.

In this study, a triangular-pitch tube bundle was used. Figure 3b shows the dimensions of the tube bundle and the locations of thermocouples on tube bundle. One thermocouple is mounted at the top dead center, the other is at the bottom dead center, and the third one is at 90 deg from the top dead center along one side of the heater tube.

2.5. Liquid collector

The liquid collector is formed from an aluminum sheet as shown in Fig. 1a. It can collect the liquid droplets bouncing from other heater tubes and the liquid film falling along the tube surface. By this collector, the dry-out phenomenon occurring on the bottom side of the heater tube can be delayed or even prevented. In addition, the overfill liquid from the liquid collector will directly drip to the top of next row tubes, see Fig. 1b. The pitch-to-diameter ratio is only 1.46 (an average value for stag-

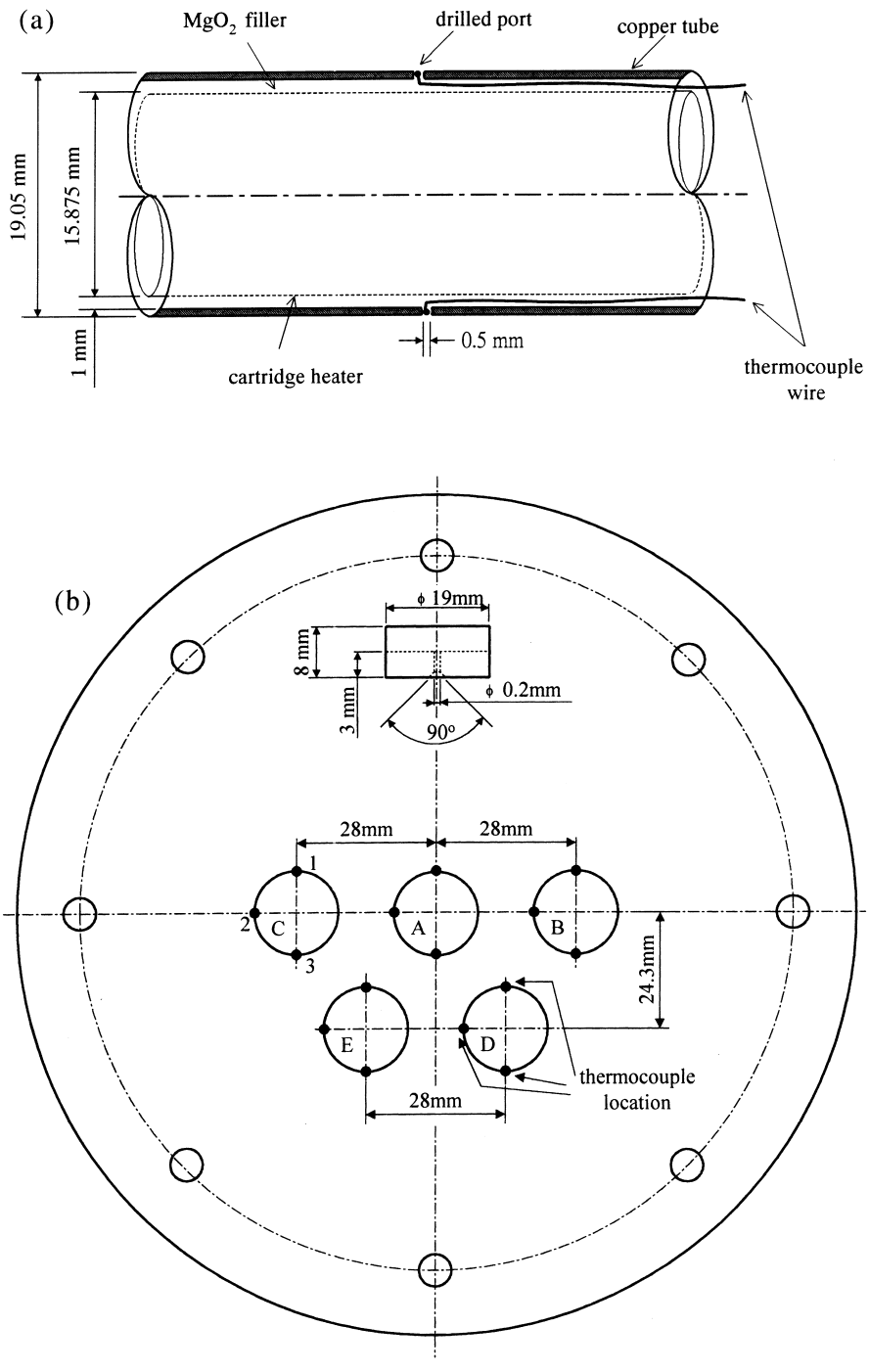

Fig. 3. (a) Schematic of heater tube. (b) Tube bundle geometry.

gered tubes), therefore, there is limited freedom to adjust the gap size between the heater tube and the collector. The gap is finally fixed at 2 mm after several sensitivity studies.

The shape of the liquid collector is simple so that it can easily be manufactured and can easily be snapped on the heater tubes. Besides, its size is only slightly larger than the tube, so it can be hanged on every tube in a compact heat exchanger.

2.6. Glycol/water flow loop

The glycol/water solution is used to cool several components of the test rig via an auxiliary flow loop. The glycol/water mixture is pumped from a chiller (with refrigeration capacity at 3 ton) to the condenser and removes the dissipated heat from refrigerant vapor. There is a closed-loop automatic temperature sensor in the chiller tank to control the temperature of the outlet glycol/water mixture at any specified temperature with an accuracy of 0.1°C.

2.7. Refrigerant

In the present work, refrigerant 141-b was used as working fluid. R141-b is a HCFC refrigerant, its advantages are non-toxic, low ODP (ozone depletion potential) and low GWP (global warming potential), so the environmental impact is relatively small. In addition, the boiling temperature at atmospheric pressure is 32°C, which is only slightly higher than room temperature. The required power to perform the boiling experiment is also low.

2.8. Data acquisition system

Data collection was carried out by a personal computer, a scanner, and a powermeter. The controlling software in the personal computer operates the powermeter and the scanner. The measured signals may be transferred to digitized readable values and displayed on the monitor. The collected and reduced information can be saved on a disk for further data reduction.

3. Experimental procedure

Before the test begins, the pump was operated at a relatively higher speed such that the stagnant air existing in the piping system can be pushed out. A vacuum pump was then used to evacuate the accumulated air from the chamber. The sprayed flow rate was controlled by a modulating bypass valve. While the bypass valve was fully opened, the regulating procedure can still be controlled via the throttling valve located prior to the exit nozzle. Increasing the nozzle inlet pressure will increase the flow rate, the refrigerant flow rate was measured by a rotameter, a commonly used flow-measurement device. The rotameter was calibrated by a mass flowmeter which was manufactured by Micro-Motion Company with an accuracy of $\pm 0.5\%$.

Each data point was obtained by averaging at least ten data-acquisition scans. To ensure the accuracy, data points were taken only at steady-state, the condition of steady-state was defined as the variation of the system saturation temperature less than 0.1°C/min.

In order to examine the influence of heat flux on heat transfer performance, the range of heat fluxes in the test was varied from below 10^4 W/m^2 to higher than $1.5*10^5$ W/m^2. During the test, if any one of the measured heater temperatures sharply increases, the input power will be turned-off to protect the instruments.

3.1. Experimental data reduction

The experimental data were reduced by a computer program which will translate and calculate the measured quantities such as nozzle pressure, chamber pressure, surface temperature, mass flow rate to become the important heat transfer parameters. The equation for the surface heat flux is

$$q'' = \frac{Q_h}{A} \tag{1}$$

where q'' is the wall heat flux (kW/m^2), Q_h the total cartridge heater power (kW), A the total surface area with power (m^2).

The average shell-side heat transfer coefficient is based on Newton's cooling law which is

$$\bar{h} = \frac{q''}{\bar{T}_w - T_s} \tag{2}$$

where $\bar{h}$ is the average shell-side heat transfer coefficient (kW/m^2 K), $\bar{T}_w$ the average wall temperature (°C), T_s the saturation temperature in the test section (°C).

The average wall temperature was taken by the arithmetic average of the thermocouple readings

$$\begin{aligned}\bar{T}_w = (&T_{A,1} + 2T_{A,2} + T_{A,3} + T_{B,1} \\ &+ 2T_{B,2} + T_{B,3} + T_{C,1} + 2T_{C,2} + T_{C,3} + T_{D,1} \\ &+ 2T_{D,2} + T_{D,3} + T_{E,1} + 2T_{E,2} + T_{E,3})/20\end{aligned} \tag{3}$$

where the subscripts A, B, C, D, E in eq. (3) represent different heaters, a thermocouple is located about 15 mm from the center-section, and about 3 mm above the nozzle height. The resulting measurements are nearly at the saturation temperature, therefore, the saturation temperature is used in the calculation of the heat transfer coefficient, i.e. T_s in eq. (2) is the saturation temperature.

3.2. Instrumentation accuracy

To ensure the accuracy of the measured data, the calibration for each measuring device must be done. The

Table 1
Instrumentation accuracy

Sensor	Accuracy
RTD, TC (temperature)	±0.2°C
Powermeter	±0.2%
Flow meter	±0.01 l/min
Pressure sensor	±0.25%

temperature sensors (RTD and thermocouples) were calibrated by a quartz thermometer which has 0.01°C accuracy. The flow meter was calibrated by a mass flow meter which has an accuracy within 8%. Other measuring devices all had the factory reports. A summary of the instrumentation accuracy for this experimental setup is shown in Table 1.

3.3. Experimental uncertainty

The propagation-of-error method [16] was used to estimate the experimental uncertainty for the average shell-side heat transfer coefficient. From eq. (2), the uncertainty in the shell-side heat transfer coefficient can be written as:

$$\delta\bar{h}=\left[\left(\frac{\partial\bar{h}}{\partial q''}\delta q''\right)^2+\left(\frac{\partial\bar{h}}{\partial\bar{T}_w}\delta\bar{T}_w\right)^2+\left(\frac{\partial\bar{h}}{\partial\bar{T}_s}\delta\bar{T}_s\right)^2\right]^{1/2} \tag{4}$$

the various terms in eq. (4) are

$$\frac{\partial\bar{h}}{\partial q''}=\frac{1}{\bar{T}_w-T_s} \tag{4a}$$

$$\frac{\partial\bar{h}}{\partial\bar{T}_w}=\frac{-q''}{(\bar{T}_w-T_s)^2} \tag{4b}$$

$$\frac{\partial\bar{h}}{\partial T_s}=\frac{q''}{(\bar{T}_w-T_s)^2} \tag{4c}$$

and $\delta q''$ is the uncertainty of the heater power, $\delta\bar{T}_w$ the uncertainty of the average temperature of the tube surface, δT_s the uncertainty of the saturation temperature of the refrigerant.

The parameter $\delta q''$ is 1% of the reading from the powermeter. Since the highest surface temperature of the heater tube is about 45°C (25 K above T_{sat}) in our tests except the dry-out cases, the estimated radiation heat loss from heater tube surface to the housing is less than 150 W/m^2, while the heat flux emitted from heater tube surface is in the range of 10^4–1.5×10^5 W/m^2. The parameters $\delta\bar{T}_w$ and δT_s can be estimated by using eq. (3) and Table 1. The experimental uncertainty for the average shell-side heat transfer coefficient can then be estimated to be about ±7%.

4. Results and discussion

Both spray evaporation and pool boiling heat transfer results are presented in Figs 4–8 for spraying R-141b on a horizontal tube and a tube bundle. The tests consisted of pure refrigerant only and the saturation temperature for all tests was controlled at 20°C.

4.1. Comparison of present data with other results

The results of a single tube pool boiling were compared to the pool boiling correlation presented by Cooper [17]. The Cooper's correlation, shown in eq. (5) below, includes the term R_p to account for the micro-roughness of the surface

$$h_{nb}=90(q'')^{0.67}M^{-0.5}P_{cr}^{n}(-\log_{10}P_{cr})^{-0.55} \tag{5}$$

where $n=0.12-0.21\log_{10}R_p$, R_p stands for surface roughness with the unit of μm.

The roughness of our copper tubes was not actually measured. According to Stephan and Abdelsalam's [18], however, the value of R_p for commercial polished copper tube was estimated to be 0.1–0.4 μm. In Fig. 4, $R_p=0.1$ and 0.4 μm are plotted to compare the present results. Other parameters used in Cooper's correlation are listed in Table 2. The present data fall within the range of Copper's correlation. The slope of the present heat transfer coefficient looks smaller than that of Cooper's correlation. The possible reason for this phenomenon may be due to the extremely good surface wettability of R-141b. For liquids with very good wettability on the heated surface usually have a relayed-boiling-inception and it also results in a lower critical heat flux.

4.2. Spray cooling data without liquid collector

The spray cooling heat transfer performance for each individual tube without liquid collector is shown in Fig. 5. We can see that heat transfer coefficient of tube A is higher than tubes B, C and tubes D, E have the lowest heat transfer coefficients. Since the nozzle was installed directly above tube A and the spray was slightly con-

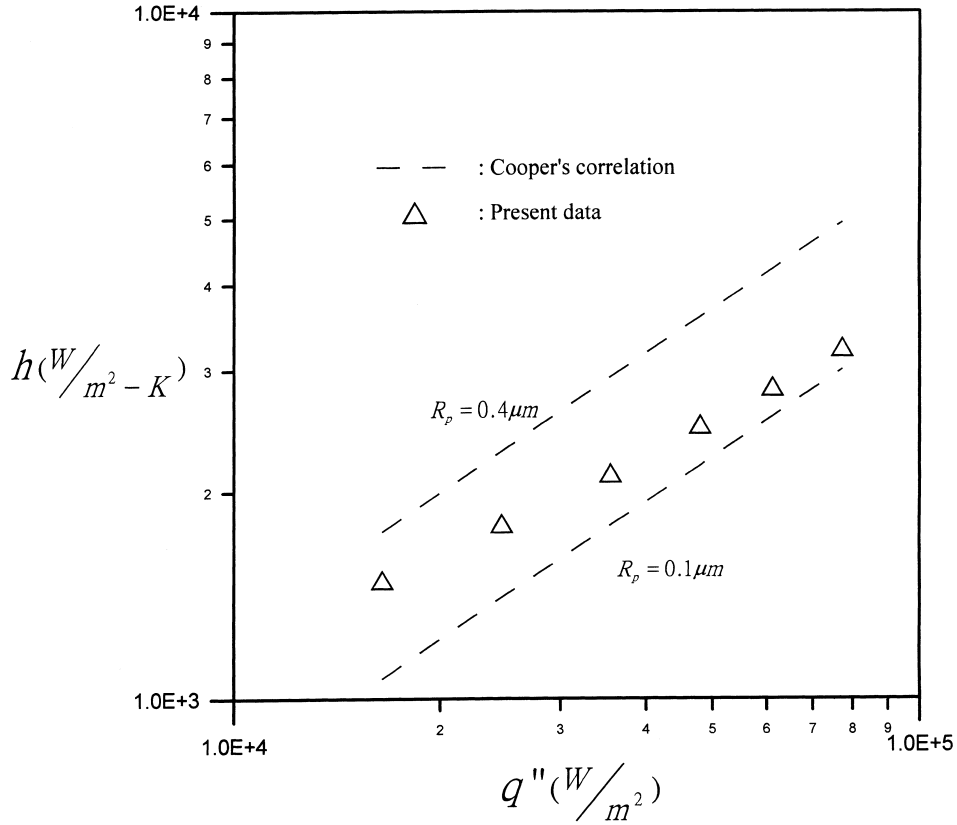

Fig. 4. Comparison of pool boiling heat transfer.

centrated around the center point of the round jet, more direct-impact sprays could be able to hit tube A than tubes B, C, while tube D and tube E received the least direct impact. As expected, the heat transfer coefficient becomes better when heat flux (or temperature difference) increases. However, when the heat transfer coefficient is beyond 3.0×10^3 W/m^2 K, the heat transfer coefficients of lower tubes begin to turn around while the heat transfer coefficients of the upper row tubes are still going up.

The above results indicate the lower tubes were unable to receive enough liquid and parts of their surfaces were drying out. From the glass-view port, we could see the bottom surfaces of tubes D, E were indeed much drier than the bottom surfaces of other tubes.

The overall heat transfer performance of the tube bundle is shown in Fig. 6. Two mass flow rates were used in the test, and the data of pool boiling data with the same test conditions are also plotted in the same figure, we can see when the surface heat flux is low (say lower than 10^4 W/m^2) the heater tubes all get enough liquid, the spray heat transfer coefficients are better than pool boiling and only weakly dependent on the spray mass flow rate. Parken et al. [19] and Moeykens and Pate [11] also observed similar results.

As the heat flux becomes higher, the probe temperature at the bottom side started to increase sharply. Which indicated that the dry-out phenomenon had occurred at the bottom side of the tube. In the consequence, the overall heat transfer coefficients and maximum heat fluxes of spray evaporation begin to fall below the pool boiling data. This maybe the reason why spray evaporation is not popular for the application of shell and tube heat exchangers or some other compact heat exchangers.

In this experiment, most of the sprayed liquid will directly impact on heater tubes. However, there a certain amount of liquid-spray did not directly impact on the heater tubes which included the liquid shooting to the right of tube B, to the left of tube C, and liquid passing between tube B and tube D as well as that between tube C and tube E.

As we have mentioned before, the spray pattern was not quite uniform, the sprayed liquid droplet is bigger and denser near the jet center. It is therefore difficult to estimate exactly how much percentage of the sprayed liquid did encounter the direct impaction.

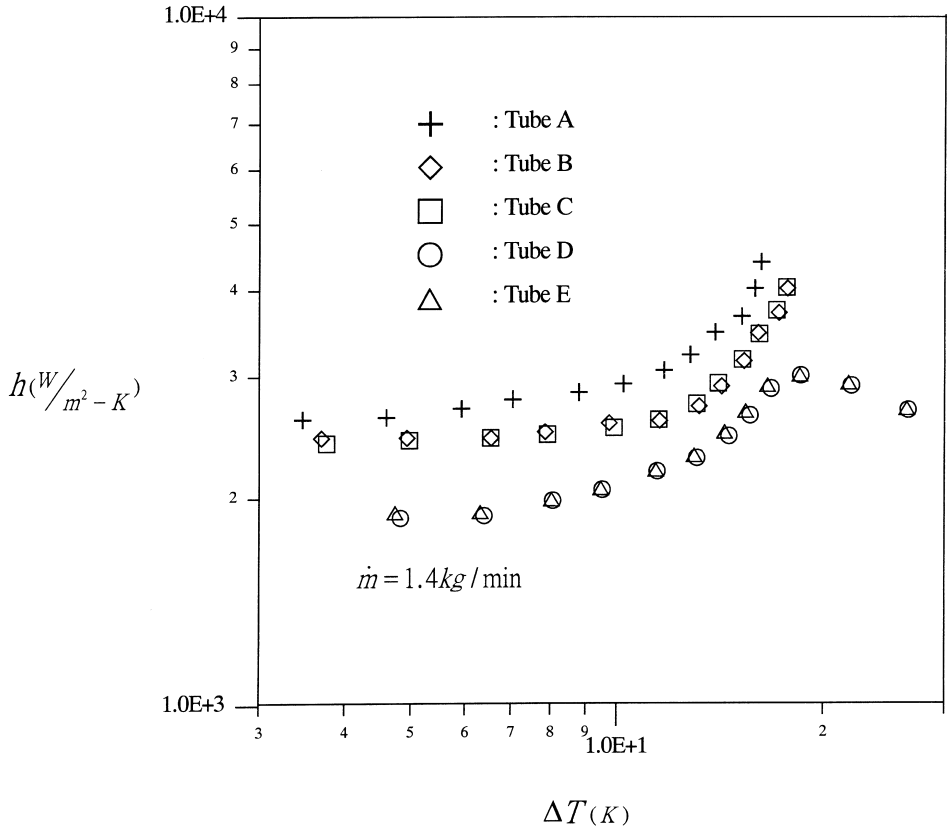

Fig. 5. Heat transfer performance of each individual tube without liquid collector.

Depending on the impact momentum and angle, the direct impacting droplet may either break into many finer droplets and bounce back and forth among surfaces or adhere on the surface and gradually fall downward.

When the surface heat flux is low, all of the tube surface is wet. Direct impaction plays the solo important role in the cooling enhancement. The excess liquid has very little contribution to the cooling. The heat transfer performance is thus insensitive to sprayed flow rate. On the other hand, when the surface heat flux is high, it should be the amount of liquid which adheres on the bottom side of heater tube that determines the onset of dry-out. The heat transfer performance is certainly sensitive to the sprayed flow rate. Although the passing liquid (which does not contact the heater surface at all), should barely participate in heater tube cooling because the vapor temperature is very close to saturation temperature.

4.3. Spray cooling performance with liquid collector

Since the dry-out phenomenon will first occur on the bottom surfaces of heater tubes when the surface heat flux is high, in this study, a liquid collector is designed to catch the liquid that bounces from other surfaces and that falls along its own tube surface.

Figure 7 shows the heat transfer performance of each individual tube in the tube bundle. We can see tube A has the highest heat transfer coefficient, this is similar to the previous case since the nozzle was installed directly above tube A, which receives more direct impaction. This time, however, the heat transfer coefficients of the other four tubes are all improved especially the lower two tubes. These results indicate the use of liquid collector can clearly impede the dry-out phenomenon.

The boiling heat transfer characteristics of the portion which is covered by liquid collectors becomes more complicated, and many studies were conducted to investigate this kind of topic, such as Chyu and Zaidi [21], Xia et al. [22] etc. When the boiling space is small relative to bubble sizes, bubble growth and departure will be affected by the walls. For examples, bubbles may be squeezed by the walls and flatter out, bubbles may coalesce, the film may be torn to pieces and eventually form the dry patches. Of course, the surrounding liquid may then flow into the dry path area and repeat the wetting and drying cycle.

Since the boiling heat transfer characteristics in a nar-

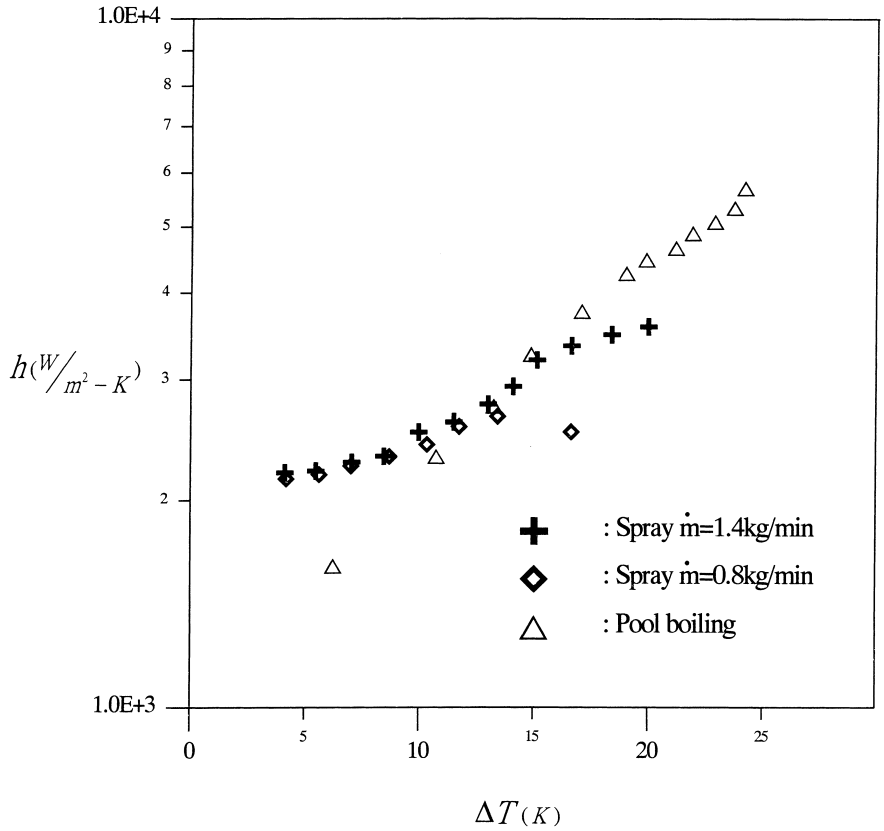

Fig. 6. Comparison of overall heat transfer without liquid collector.

row gap is so dynamic, the above mentioned scenario hardly explains all of the possible heat transfer mechanisms. In fact, Chyu and Zaidi [21] found the local temperature of nucleate boiling in a narrow gap had a wide range of variation even under the same test conditions. In our tests, the power was turned off when the first sharp rise in temperature is detected. Therefore, the dry patch had not yet prevailed. The wide variation in local temperature was not detected in the study. The critical heat fluxes obtained in this study may thus be slightly conservative.

Figure 8 shows the differences of the overall heat transfer coefficients with and without liquid collector under the same spray rate. For comparison purpose, pool boiling data are also presented in the same figure. The results show that spray cooling with liquid collectors has the best heat transfer coefficients in the whole range of test conditions.

At moderate heat flux, the heat transfer performances of both spray cases are much better than pool boiling data. However when the heat flux becomes higher, only the case with liquid collector can surpass pool boiling data. The maximum heat flux (before CHF occurs) and the corresponding heat transfer coefficient can exceed 30% more than pool boiling data. Many other factors, such as the use of a better spray pattern and the change of gap size etc., should be able to improve the heat transfer performance.

5. Conclusions

The present test shows the heat transfer performance of spray evaporation on a staggered tube bundle. The simple liquid collector is designed to clip on each tube of the bundle. With this simple modification, the dry-out phenomenon occurring on the bottom surface of the tube can be delayed, this kind of CHF delay allows much larger heat fluxes to be extracted from the heater tube surfaces. Therefore, the overall heat transfer coefficient can be significantly improved. The liquid collector is easy to manufacture and easy to install at low cost. It can be replaced regularly at the maintenance period if the potential scale could accumulate on it. Therefore, this kind of modification should be suitable for a compact

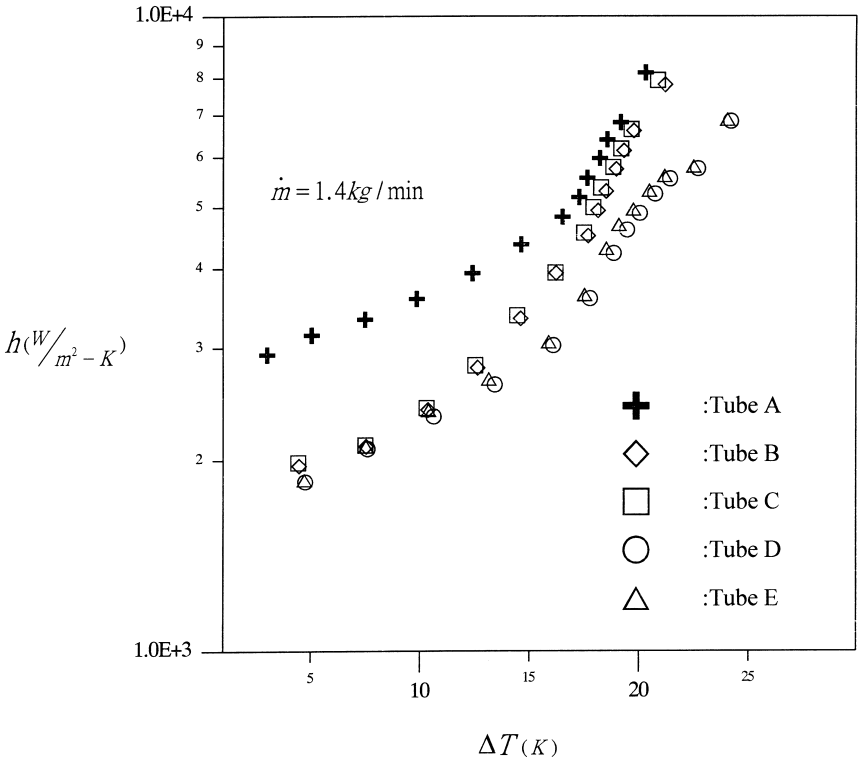

Fig. 7. Spray evaporation data of each individual tube with liquid collector.

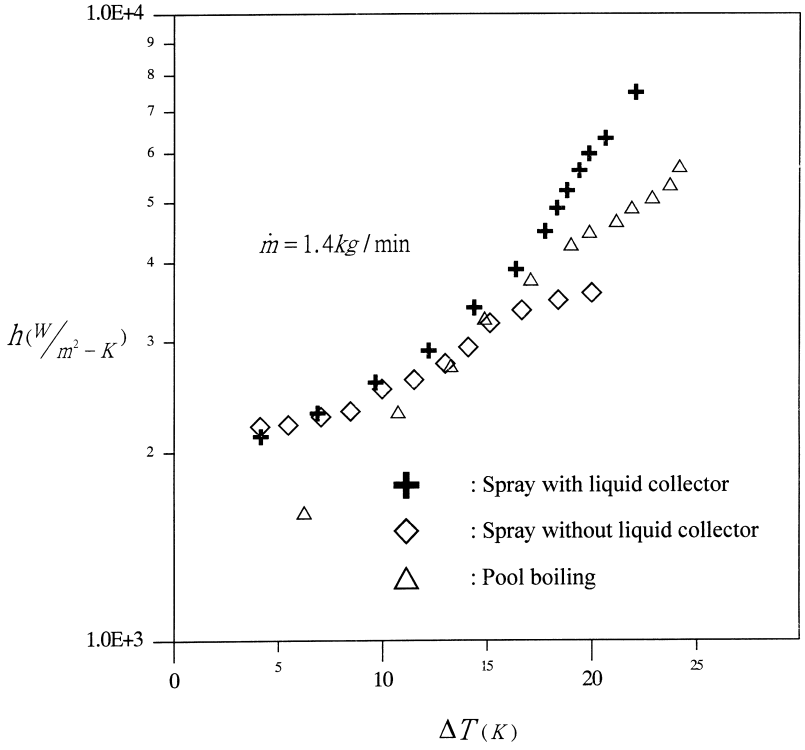

Fig. 8. Comparison of overall heat transfer (with and without liquid collector).

Table 2
Properties and operated conditions of R-141b test

Refrigerant 141b		
M	molecular weight	117
P_c	critical pressure	4.12 MPa
P	saturation pressure (at 20°C)	0.065 MPa
P_{cr}	P/P_c	0.01578

shell and tube heat exchanger with the addition of top spray cooling.

Acknowledgement

Financial support for this study provided by the National Science Foundation of Taiwan is greatly appreciated.

References

[1] M.R. Pais et al., Surface roughness and its effects on the heat transfer mechanism in spray cooling, J. Heat Transfer 144 (1992) 211–219.
[2] G.P. Celata, A review of recent experiments and predictions aspects of burnout at very high heat fluxes, Proceedings of The International Conference on Multiphase Flows, Tsukuba, Japan, Sept. 24–27, 1991.
[3] X. Lin, J.H.V. Lienhard, Extremely high heat fluxes beneath impinging liquid jets, ASME J. Heat Transfer 115 (1993) 472–476.
[4] J.W. Hodgson, J.E. Sutherland, Heat transfer from a spray cooled isothermal cylinder, Industrial and Engineering Chemistry, Fundamentals 7 (1968) 567–571.
[5] K.J. Choi, S.C. Yao, Mechanisms of film boiling heat transfer of normally impacting spray, Int. J. Heat and Mass Transfer 30 (2) (1987) 311–318.
[6] M.R. Pais, L.C. Chow, E.T. Mahefkey, Surface roughness and its effects on heat transfer mechanism in spray cooling, ASME J. Heat Transfer 114 (1992) 211–219.
[7] S. Deb, S.C. Yao, Analysis on film boiling heat transfer of impacting sprays, Int. J. Heat and Mass Transfer 32 (11) (1989) 2099–2112.
[8] M.C. Chyu, A.E. Bergles, Enhancement of horizontal tube spray film evaporators by structured surfaces, 23rd National Heat Transfer Conference, Denver, 1985.
[9] M.C. Chyu, A.E. Bergles, Falling film evaporation on a horizontal tube, 23rd National Heat Transfer Conference, Denver, 1985.
[10] M.C. Chyu, A.E. Bergles, Horizontal-tube falling-film evaporation with structured surfaces, ASME J. Heat Transfer 111 (1989) 518–524.
[11] S.A. Moeykens, M.B. Pate, Spray evaporation heat transfer of R-134a on plain tubes, ASHRAE Trans. 100 (1995) 173–184.
[12] S.A. Moeykens, M.B. Pate, The effects of nozzle height and orifice size on spray evaporation heat transfer performance for a low-finned, triangular-pitch tube bundle with R-134a, ASHRAE Trans. 101 (1996) 420–433.
[13] K.R. Chun, R.A. Seban, Performance prediction of falling film evaporators, ASME J. Heat Transfer (1972) 432–436.
[14] M.C. Chyu et al., Enhancement of horizontal tube spray film evaporators, heat transfer, Proceedings of the 7th International Heat Transfer Conference, Munich, 6, 1982, pp. 275–580.
[15] J.R. Thome, Two phase heat transfer to new refrigerants, Proceedings of 10th International Heat Transfer Conference, 1, 1994, pp. 19–41.
[16] J.P. Holman, Experimental Methods for Engineers, McGraw-Hill, New York, 1994, pp. 49–62.
[17] M.G. Cooper, Saturation nucleate pool boiling: a simple correlation, International Chemical Engineering Symposium, Ser. 86, 1984, pp. 785–792.
[18] K. Stephan, M. Abdelsalam, Heat-transfer correlations for natural convection boiling, Int. J. Heat and Mass Transfer 23 (1980) 73–87.
[19] W.H. Parken et al., Heat transfer through falling film evaporation and boiling on horizontal tube, ASME J. Heat Transfer (1990) 744–750.
[20] C.R. Tong, M.J. Tan, S.G. Bankoff, Model for convective boiling in a narrow eccentric annular gap, J. Eng. Gas Turbines and Power, Trans. ASME 107 (3) (1985) 613–619.
[21] M.C. Chyu, S.H.R. Zaidi, Characteristics of boiling heat transfer in a narrow gap, Winter Annual Meeting of the American Society of Mechanical Engineers, Dallas, 1990.
[22] C.L. Xia, Z.Y. Guo, W.L. Hu, Mechanism of boiling heat transfer in narrow channels, 28th National Heat Transfer Conference, San Diego, 1992.